ACSNANO
www.acsnano.org
ARTICLE

Phage-Based Structural Color Sensors and Their Pattern Recognition Sensing System

Ju Hun Lee,[†,‡] Benson Fan,[§] Tuan D. Samdin,[∥] David A. Monteiro,[†,⊥] Malav S. Desai,[†,‡] Olivia Scheideler,[†,‡] Hyo-Eon Jin,[†,‡,▲] Soyoun Kim,[#] and Seung-Wuk Lee*[,†,‡,¶]

[†]Department of Bioengineering, University of California, Berkeley, California 94720, United States
[‡]Biological Systems and Engineering, Lawrence Berkeley National Laboratory, Berkeley, California 94720, United States
[§]Bioinspira Inc., Berkeley, California 94720, United States
[∥]Department of Molecular and Cell Biology, University of California, Berkeley, California 94720, United States
[⊥]University of California, Berkeley−University of California, San Francisco Graduate Program in Bioengineering, University of California, Berkeley, California 94720, United States
[#]Department of Biomedical Engineering, Dongguk University, Seoul 04620, Republic of Korea
[¶]Tsinghua−Berkeley Shenzhen Institute, Shenzhen, People's Republic of China
[▲]College of Pharmacy, Ajou University, Suwon 16499, Republic of Korea

Supporting Information

ABSTRACT: **The mammalian olfactory system provides great inspiration for the design of intelligent sensors. To this end, we have developed a bioinspired phage nanostructure-based color sensor array and a smartphone-based sensing network system. Using a M13 bacteriophage (phage) as a basic building block, we created structural color matrices that are composed of liquid-crystalline bundled nanofibers from self-assembled phages. The phages were engineered to express cross-responsive receptors on their major coat protein (pVIII), leading to rapid, detectable color changes upon exposure to various target chemicals, resulting in chemical- and concentration-dependent color fingerprints. Using these sensors, we have successfully detected 5−90% relative humidity with 0.2% sensitivity. In addition, after modification with aromatic receptors, we were able to distinguish between various structurally similar toxic chemicals including benzene, toluene, xylene, and aniline. Furthermore, we have developed a method of interpreting and disseminating results from these sensors using smartphones to establish a wireless system. Our phage-based sensor system has the potential to be very useful in improving national security and monitoring the environment and human health.**

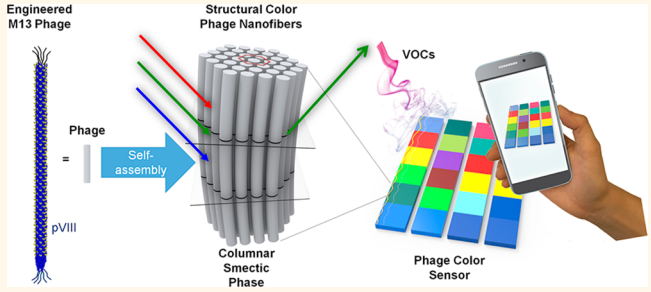

KEYWORDS: *M13 bacteriophage, columnar smectic phase, cross-reactive, structural color, biomimetics, biosensor, olfactory system*

Advanced sensor systems are invaluable for numerous applications in the environment, national defense, and healthcare. Designing a next generation sensor system requires taking accuracy, repeatability, stability, miniaturization, cost, and ease-of-use into consideration. Although various chemical, optical, and electronic sensors have been demonstrated in controlled environments,[1−4] development of a sensor system for desired target analytes in ambient conditions is still challenging. In nature, the mammalian olfactory system is an excellent example of molecular recognition and provides great inspiration to design such a sensor. The mammalian olfactory system is highly sensitive and selective and can detect and distinguish between a broad range of chemicals.[5] This ability is possible due to the cross-reactivity of olfactory epithelial cells that generate chemical- and concentration-dependent signals coupled with the brain's capacity for pattern recognition.[6−11] In order to mimic the mammalian's olfactory system, several man-made materials have been utilized to construct electronic noses and tongues for chemical pattern recognition.[12−23] Arrays of colorimetric dyes and electric and optical sensors have been demonstrated to detect various volatile organic chemicals (VOCs) or characteristic marker gases for disease diagnostics.[24−33] Despite significant technical advances in sensor development, we still rely on canine screening to detect various explosives and drugs in our daily life.[34,35] It is still challenging

Received: November 26, 2016
Accepted: March 29, 2017
Published: March 29, 2017

DOI: 10.1021/acsnano.6b07942
ACS Nano 2017, 11, 3632−3641

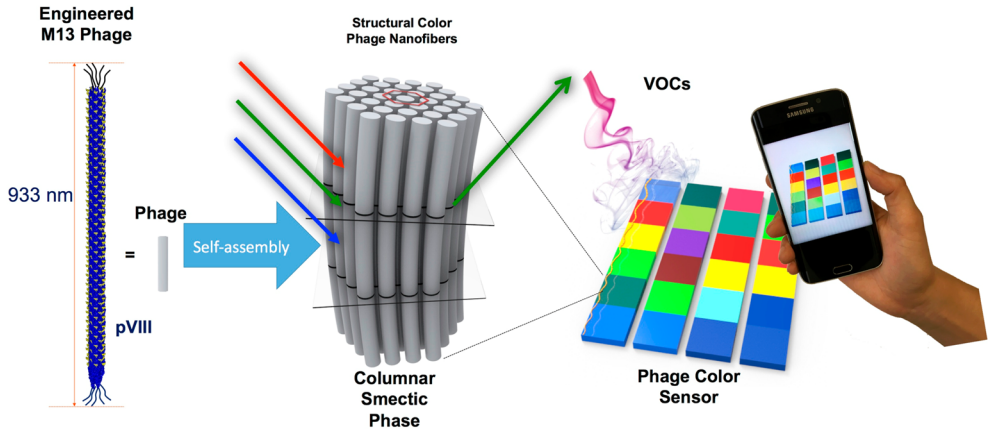

Figure 1. Schematic illustration of phage structural color sensors. M13 phages were engineered to contain cross-reactive receptors on their major coat protein (pVIII) that can interact with various target analytes. The phages were assembled into hierarchical bundled nanostructures in a columnar smectic phase. The resulting nanostructures can scatter visible light and exhibit brilliant colors, which we exploited for color sensors. The phage color sensors exhibited rapid, detectable color changes upon exposure to various target chemicals, resulting in a chemical- and concentration-dependent manner. We can fabricate arrays of these matrices which can be analyzed and the results disseminated using smartphones and a wireless network system. The image of Samsung Galaxy is used with permission from Samsung Electronics Co., Ltd.

to develop sensitive, selective, and easy-to-use sensors for desired target chemicals. Here, we demonstrate a sensitive and selective color sensor that utilizes M13 bacteriophage (phage) structural matrices and an accompanying smartphone-based sensing system (Figure 1). We first genetically engineered multiple distinct functional groups on the phage major coat proteins. We then exploited the phage to self-assemble into hierarchical nanostructures composed of columnar smectic phase nanofibers using surfactant-assisted self-assembly at the interface between liquid, solid, and air (meniscus). The resulting phage matrices exhibited detectable color changes in the presence of different amounts of relative humidity that could be tuned by varying the bundle diameters and responded to various volatile organic chemicals. Through quantitative pattern analysis of these color changes, we were able to estimate its local percentage of relative humidity in a sensitive manner. After receptor functionalization, we selectively distinguished various toxic chemicals including benzene, toluene, xylene, and aniline. Finally, we implemented an automated sensor analysis system in real time to capture and share the sensing results through a wireless network with a smartphone (Figure 1). We believe our phage color sensor-based automated sensing system can be very useful for the development of a wearable sensor network to improve our ability to secure the environment, healthcare, and national security.

RESULTS

Fabrication and Characterization of M13 Phage Columnar Smectic Structures. We have developed structural color matrices using M13 phage self-assembled nanostructures. M13 phage is a filamentous virus that infects bacterial cells, composed of a single-stranded DNA encapsulated by 2700 copies of the pVIII major coat protein. We can display desirable receptor-like molecules on their coat protein surfaces through genetic and chemical approaches.[36−42] M13 phage is specific only to bacterial cells and benign for human beings and animals, which make them safe for use in practical applications.[43] Large quantities of identical phage are easily prepared through bacterial amplification.[39] M13 phage can also tolerate various environmental conditions including extreme pH, elevated temperatures, chaotropic agents, and high ionic concentration.[44,45] Therefore, M13 phage is a great candidate as a sensor-fabricating material. We recently developed a self-assembly process to create a variety of biomimetic nanostructures, which we termed a self-templating process.[46] Using the self-templating assembly of phages, we can easily prepare biomimetic nanostructures similar to those of collagen, chitin, and cellulose that can form hierarchically organized structures in nature. Among them, the self-templated phage films with bundled nanostructures exhibited structural colors similar to those observed in avian skin collagen.[47,48]

Our phage matrices are composed of columnar smectic phage nanofibers that were created through the use of a surfactant-driven depletion force during the self-templating process (Figure 2). Especially critical for the creation of highly controlled self-assembled nanostructures is the absence of phage aggregates in solution. To this end, we used a surfactant (polyoxyethylene sorbitan monolaurate, Tween20) to stabilize the phage particles and keep them evenly dispersed in Tris-buffered saline (TBS). When we developed phage nanostructures using Tween20 during the self-templating process, we observed an additional effect of the surfactant. Interactions between the phage particles and the surfactant induce depletion forces entropically and enable the creation of a variety of nanostructures. We discovered a columnar smectic liquid-crystal phase, which possesses combinatorial properties of two distinct phases—smectic phase and columnar phase. Specifically, similar to the smectic phase, the assembled phages are parallelly aligned and arranged in layers, with the axis of alignment perpendicular to the layer plane. Concurrently, we also observe columnar phase characteristics as the phages are oriented with a high volume fraction (above the smectic range) and are hexagonally packed. In general, system parameters such as temperature and concentration guide the sequential liquid-crystal phase transition from an isotropic phase to nematic, smectic, columnar, and crystalline phases;[49,50] however, the presence of surfactants at the meniscus during the self-templating process enables the generation of columnar smectic phase. During the self-templating process, solvent evaporation at the air−liquid−solid interface (meniscus) increases both surfactant and phage concentration near the meniscus. Higher

DOI: 10.1021/acsnano.6b07942
ACS Nano 2017, 11, 3632−3641

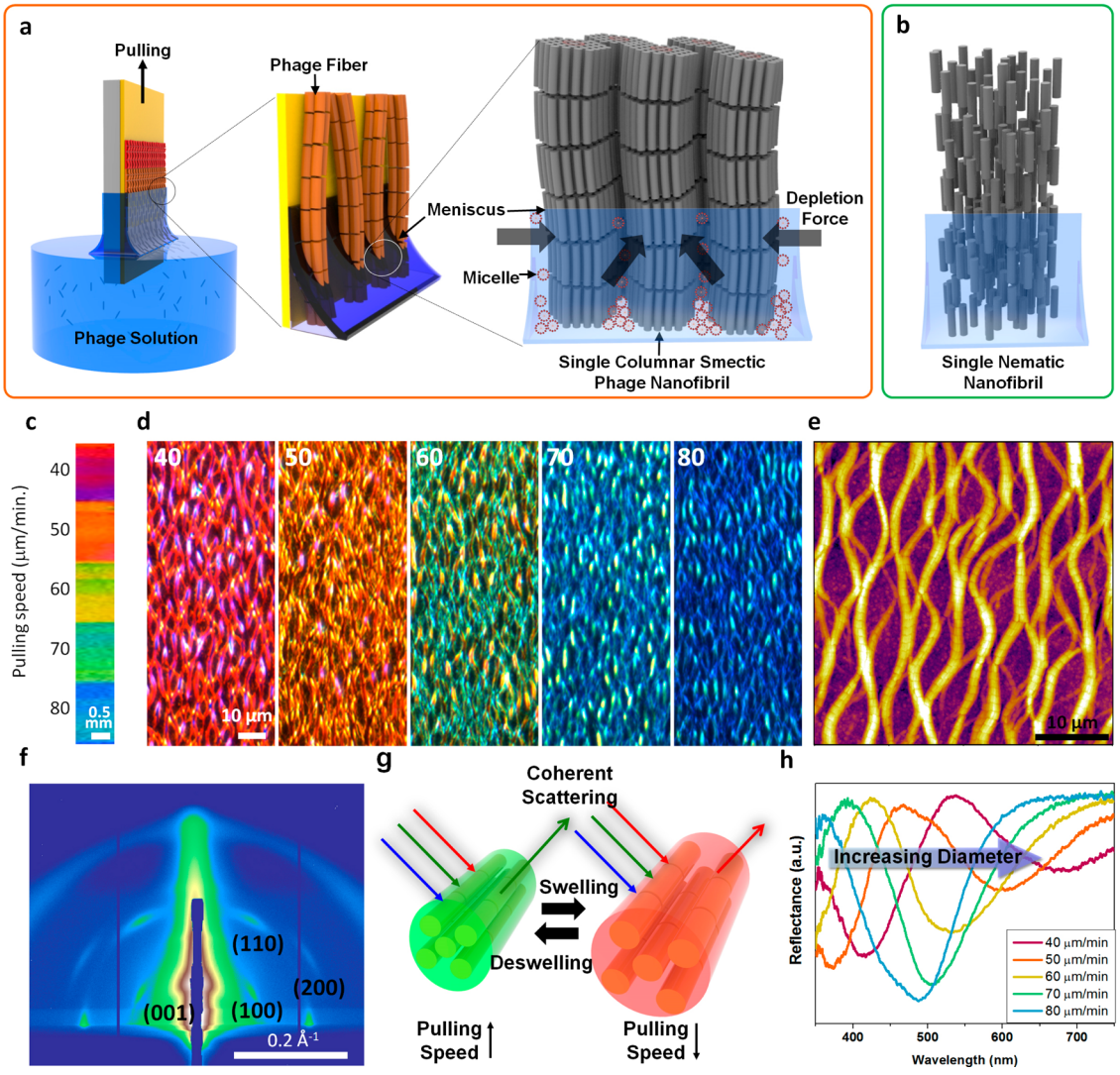

Figure 2. Characteristics of representative columnar smectic phage nanostructures. (a) Schematics of columnar smectic phage nanostructure synthesis. During the self-assembly process, surfactant micelles can induce a depletion force (black arrows) to increase phage packing density and assembly into an ordered bundled nanofiber phase. (b) Schematic illustration of the nematic phase that is induced in the absence of surfactant. (c) Photograph of color film made from M13 phage engineered with four glutamate (4E) groups onto the major coat protein, developed with varying pulling speeds to exhibit distinct colors. (d) Dark-field optical microscope images of hierarchically bundled 4E phage films to show scattered light from the phage bundles. Pulling speed of each image: 40, 50, 60, 70, and 80 μm/min. (e) AFM image of columnar smectic 4E phage bundles. (f) Grazing-incidence small-angle X-ray scattering characterization of the M13 phage structural color film. (g) Schematic illustration of the coherent scattering of the light on the columnar smectic phase phage nanofibers. With an increase in pulling speed, the bundle diameter decreases. Upon exposure to the target analyte, the bundles swell and exhibit a longer wavelength of light. (h) Reflectance spectra of the phage color films. A blue shift was observed from the reflectance spectra of the film with increase of pulling speed due to the decrease of phage bundle diameter.

surfactant concentration leads to the formation of a higher density of surfactant micelles. At the same time, the phage particle concentration also increases and they begin to organize themselves into liquid crystals in solution. Due to differences in the shape, size, and motility of the surfactant micelles and liquid-crystalline phage particles, further increases in concentration can lead to an even denser packing of phage that is entropically driven by the depletion and segregation of surfactant micelles (Figure 2a).[51−54] When we couple this phenomenon with self-templating process, we can fabricate phage nanofiber structures in the columnar smectic phase in a tunable manner (Figure 2a). In the absence of surfactant, but with the same high concentration of phage, our self-templating process results in nanofibers that exist in the conventional nematic phase (Figure 2b). Our results suggest that the major driving force that enables formation of columnar smectic phase nanofibers over nematic phase nanofibers is the enhanced, entropically driven depletion force enabled by the surfactant. By varying the pulling speed during the self-templating process, we were able to create a variety of phage color matrices by altering the diameter of bundled nanofibers and their distribution in the matrices. The resulting phage matrix exhibited a wide range of brilliant colors (Figure 2c). Dark-field optical microscopy images showed that the resulting phage coherently scattered different wavelengths of light depending on the diameter of the bundled nanostructures (Figure 2d). Atomic force microscopy (AFM) analysis showed that the brilliantly colored phage films were composed of bundled

DOI: 10.1021/acsnano.6b07942
ACS Nano 2017, 11, 3632−3641

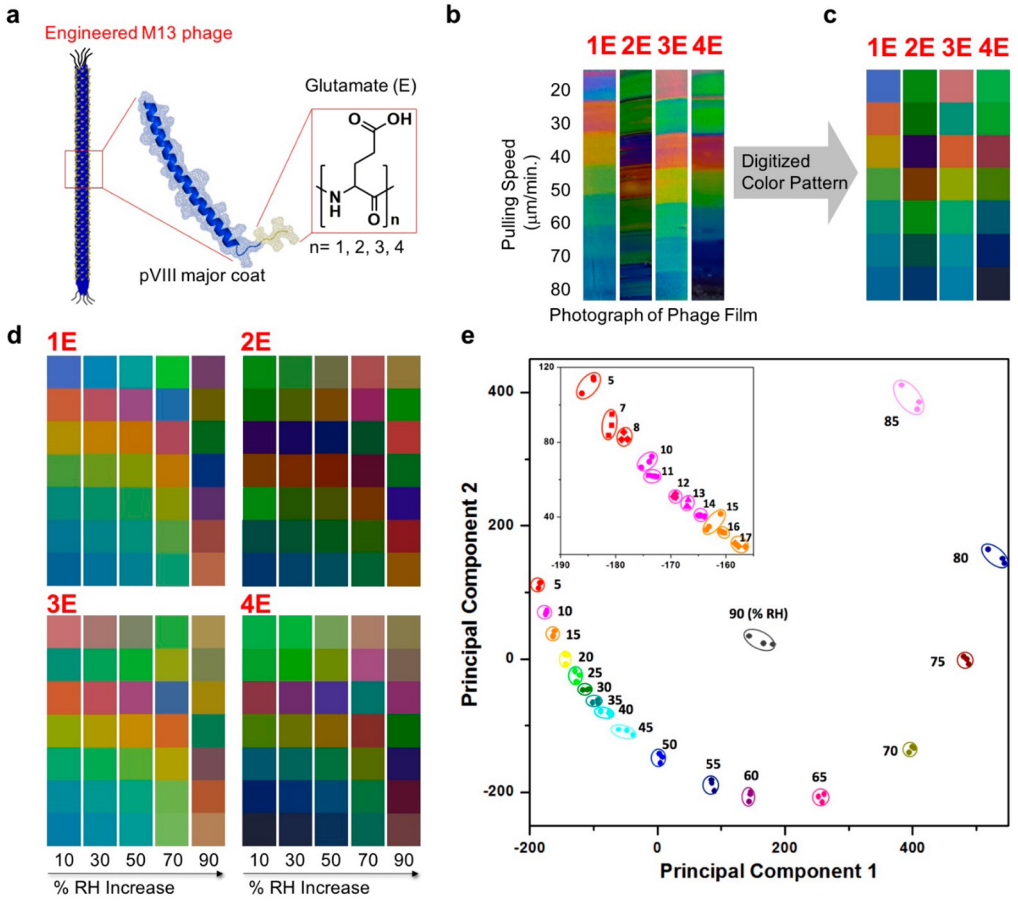

Figure 3. Phage color sensor arrays for relative humidity (% RH) sensing. (a) Schematic of genetically engineered M13 phage with glutamate (E) modifications at the N-termini of the surface coat protein (pVIII). (b) Photographs of M13 phage structural color array. 1E/2E/3E/4E indicate the number of glutamates added to each coat protein. (c) Digitized color patterns of the phage color matrices. Four different kinds of engineered phage and seven different pulling speeds were used to make a 28-matrix array for humidity sensing. (d) Phage color patterns generated from 1E, 2E, 3E, and 4E phage when they were exposed to different amounts of humidity between 10 and 90% RH. (e) Principal component analysis of the color changes resulting from the exposure of the phage color arrays to 5−90% RH with 5% RH increments. Inset figure shows that phage sensors and an analysis tool can sensitively discern 1% difference in relative humidity (5−17% RH).

smectic nanofibers (Figure 2e). Each nanofiber structure consisted of multiple columnar smectic phase nanofibrils of phage (Figure 2a and Supporting Information Figure S1a,b). The average length of the smectic domain was 929 ± 29 nm, which is consistent with the length of the engineered phage (933 ± 21 nm, n = 20). The resulting smectic nanofiber structures with Tween20 showed more loosely spaced nanofiber structures compared to those without Tween20 (Figure 2a,b,e and Supporting Information Figure S1c,d). Grazing-incidence small-angle X-ray scattering (GISAXS) analysis showed that the phage film exhibited high intensity peaks corresponding to (001), (100), (110), and (200) diffraction spacing (Figure 2f), indicating that the nanobundled structures possess hexagonally packed structures. In order to investigate the structure-dependent coherent scattering of the phage nanofiber, we prepared multiple columnar smectic nanofiber structures with different diameters by controlling the pulling speed. AFM analysis showed that with increasing pulling speed, the diameter of phage nanofiber decreased (Supporting Information Figures S2 and S3). The optical images and reflectance spectra showed that the coloration of phage film is strongly dependent on the morphology of the bundled structures (Figure 2c,d,h). The nanostructures with a larger diameter exhibited a longer wavelength of light, whereas those with smaller diameters exhibited a shorter wavelength. We believe that multiple highly crystalline columnar smectic single-phage nanofibrils (on the order of hundreds of nanometers) and their spatial distribution inside a hierarchical (larger) phage nanofiber induce coherent scattering to generate brilliant color from hierarchical phage fibers. Therefore, the addition of surfactant stabilizes the phage homogeneous suspension to prevent aggregation and to help produce highly tunable fibrous columnar smectic phases at the meniscus during the self-templating process.

Phage Color Sensors for Sensitive Humidity Detection. The resulting phage films exhibit highly sensitive color changes in the presence of varying amounts of humidity. The detection and quantification of moisture in air is critical in various applications.[55,56] In order to validate the ability of our phage color sensor to detect humidity (relative humidity, RH) in a sensitive manner, we genetically engineered M13 phage with multiple glutamate (E) groups on their major coat protein (pVIII), specifically E, 2E, 3E, and 4E (Figure 3a). These distinct phage populations possess different surface charges and hydrophilic properties and thus exhibit distinct color changes. We exploited these phages to self-assemble on gold-coated silicon substrates through the self-templating process and constructed an array of 28 distinct phage matrices that varied in

DOI: 10.1021/acsnano.6b07942
ACS Nano 2017, 11, 3632−3641

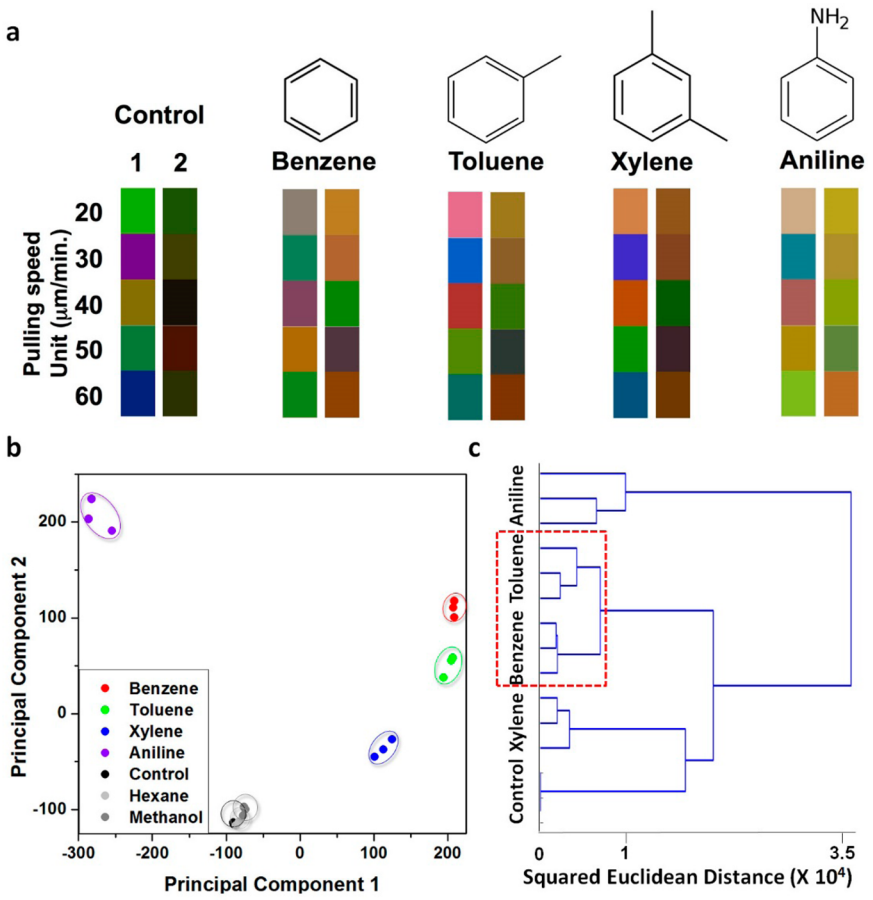

Figure 4. Phage color sensor arrays for benzene, toluene, xylene, and aniline (BTXA) sensing. (a) Aromatic phage color array made from (1) wild-type phage with chemically engineered benzoic acid residues on their major coat protein (pVIII) and (2) genetically engineered phage containing WHW peptides on their major coat protein. Using these two phage populations and a series of different pulling speeds, we compared RGB values across 10 matrices (30 dimensions). (b) Principal component analysis of the results from three separate experiments using each target analyte (*i.e.*, BTXA) and controls (ambient air, hexane, and methanol). (c) Hierarchical clustering analysis of the phage color sensors upon exposure to benzene, toluene, xylene, aniline, and control (ambient air). Euclidean distances were calculated as the distances between analyses in 30-dimensional space.

the type of phage and substrate pulling speed (Figure 3b,c). The color of each matrix in the presence of different amounts of RH was captured and analyzed for its red, green, and blue (RGB) color components using a charge-coupled device (CCD) video camera controlled by a MATLAB program in real time. In order to prevent interference from stray light during image capturing, we set up the experiment in a dark, close system with a fixed light source and a computer-controlled CCD camera (red dotted square in Supporting Information Figure S4). A program was also used to control the camera settings to the parameters set in Table S1. In addition to the controlled setup, we used a reference gray card that allowed for white balancing to significantly reduce the uncertainty depending on lighting conditions (Supporting Information Figure S5). The resulting phage color patterns (Figure 3d and Supporting Information Figure S6) confirm that the cross-reactive phage array can effectively discriminate between different levels of RH through generation of color combinations, or color fingerprints. Using this method, we are able to readily sense and distinguish between 5 and 90% RH. For quantitative analysis of the color changes, we defined 84 different array vectors [3 color components (RGB) per matrix across 28 matrices (4 different functional groups (E, EE, EEE, and EEEE) and 7 different color arrays per functional groups (generated by seven different pulling speeds))] of each humidity level from 5 to 90% RH, with 5% RH increments. These 84-dimensional vectors each correspond to a digitized color fingerprint (Figure 3). With those values, a principal component analysis (PCA) was conducted for evaluation of high reproducibility as well as determination of the number of meaningful independent dimensions in cross-reactive patterns.[24,48,57] The first two-dimensional PCA plot of RH data from 5 to 90% showed the phage color sensor could reproducibly distinguish a wide range of % RH with significant accuracy (Figure 3e). In fact, the first two principal components were able to capture 88% of the variance in the measurements. The phage color matrices could distinguish 0.2% RH difference based on three standard deviations from the baseline. We also confirmed that less than 1% RH difference in low % RH regime could be discriminated in 2D-PCA space (Figure 3e, inset). Indeed, the range of responses to stimuli with brilliant colored columnar smectic phage array films are greater compared to the responses of previous nematic phage films (Supporting Information Figure S7), allowing us to take advantage of phage films as a sensing platform. Furthermore, the response time of the phage color array, measured from 10 to 90% of the peak RGB value while switching from 5 to 80% RH, was ~80 ms (n = 3) (Supporting Information Figure S8).

DOI: 10.1021/acsnano.6b07942
ACS Nano 2017, 11, 3632–3641

Figure 5. Schematics of smartphone-based sensor analysis system. (a) Schematic of perception of smell. When odorant molecules come to the surface of an olfactory membrane, they activate multiple cross-reactive receptors that transfer a unique combination of signals through neurons to the glomeruli of the olfactory bulb (OB). Colorimetric fingerprints from cross-reactive phage color sensor arrays can be analyzed in a similar manner. Images of phage sensors that have been exposed to target analytes can be taken by a smartphone and uploaded to a server for analysis against a database of reference color fingerprints. (b) Screen captured images from Samsung Galaxy smartphone and Samsung Gear smartwatch exhibit the analytic and communication capabilities of our system during a live demonstration (Supporting Movie SM1). Through smartphones and wearable devices (*i.e.*, smartwatch or smartglasses), these results are shared *via* SMS text messages, e-mail, or on social media and include spatiotemporal information with the location and date/time that the image was captured. Previous results are stored in the server, generating a comprehensive event history. The image of Samsung Galaxy and the captured images from Samsung Galaxy and Samsung Gear are used with permission from Samsung Electronics Co., Ltd.

Phage Color Sensors for Selective Detection of Benzene, Toluene, Xylene, and Aniline. Sensitive detection and identification of benzene, toluene, xylene, and aniline (BTXA) is a critical mechanism in the petrochemical industry and for environmental protection.[58,59] For BTXA sensing, we engineered cross-reactive aromatic receptors onto M13 phages through two distinct, parallel approaches. Specifically, we genetically engineered tryptophan−histidine−tryptophan (WHW) chains onto the ends of the pVIII major coat protein and chemically added benzoic acid residues to the N-termini of pVIII proteins of the wild-type phage. The chemical functionalization approach led to the addition of approximately 1161 ± 66 (n = 3) phenyl groups per virus as confirmed by quantitative measurements with matrix-assisted laser desorption ionization time-of-flight mass spectrometry (MALDI-TOF MS, Supporting Information Figure S9).[40,60] These two distinct genetically and chemically engineered aromatic phages were separately self-assembled on substrates through self-templating. We do not observe any significant differences in the nanofiber structure between these phage and the glutamate-engineered phage (Supporting Information Figure S10). Upon exposure to these targets, RGB color changes across each array were recorded and analyzed in a manner similar to that used for % RH, and the fingerprint-like nature of the arrays enabled precise identification of specific aromatic molecules based on color change in the presence of BTXA species (Figure 4a and Supporting Information Figure S11). These results were attributed to differences in the structural changes of these matrices due to the different binding affinities of the engineered pVIII modifications to different chemical species.

A two-dimensional PCA showed that these species can be easily distinguished across repeated trials (n = 3) using the four pure target gases and controls (ambient air, hexane (aliphatic, hydrophobic), and methanol (aliphatic, polar)) (Figure 4b). In fact, the first two principal components were able to capture 97% of the variance in the measurements. Furthermore, we used hierarchical clustering analysis (HCA) to study similarities across the colorimetric fingerprints of these four analytes by comparing their closeness in 30-dimensional space. The resulting dendrogram of five samples (benzene, toluene, xylene, aniline, and control (n = 3); Figure 4c) showed that all four gases and a control could be accurately distinguished. Interestingly, the dendrogram also shows that distinct molecules with similar chemical structures appear closer in the hierarchical tree. For example, benzene and toluene differ by only one carbon and are located closest together (Figure 4c, red dashed box). We also performed experiments in mixed vapors of a single type of BTXA in combination with methanol and hexane to test the specificity of our phage sensor in the presence of interfering molecules. The results of two-dimensional PCA and HCA demonstrated that our system can selectively identify aromatic compounds even in the presence of methanol and hexane (Supporting Information Figure S12c,d). In addition, to investigate the detection limit and calibration curves of the phage color array, we tested the sensing capability of the phage array with a single gas, xylene, at different concentrations. The resulting phage color patterns could distinguish 5 ppm of xylene, which is a 20 times dilution of the permissible exposure limit level of xylene (Supporting Information Figure S13a). The detection limit was assumed to be three standard deviations from baseline noise in the absence of analytes. We also confirmed that the phage patterns could differentiate xylene gas at different concentrations, for example, from 5 to 11 500 ppm (saturated xylene vapor at room temperature, which is 13.0 times higher than immediately dangerous to life or health level of xylene) as shown in Supporting Information Figure S13b,c.

Smartphone-Based Sensor Analysis and Information Sharing. Inspired by pattern-recognition-based odor perception as seen in the mammalian olfactory system,[10,61,62] we developed a phage sensor analysis tool using smartphones and a wireless network (Figure 5a and Supporting Information Figure S14). This system requires a populated database to be used as a reference in analyzing new results. To do this, we generated the RGB colorimetric profile database of the phage sensor array when exposed to known chemicals and concentrations. When a new image is captured for analysis, its RGB colorimetric information is calculated and the results are looked-up in the database for analysis. The algorithm automatically determines the two closest records in the database and estimates the

DOI: 10.1021/acsnano.6b07942
ACS Nano 2017, 11, 3632−3641

analyte concentration by interpolation with known values. To demonstrate this analysis system, we have captured a recording of the use of a smartphone and a phage humidity color sensor (Supporting Movie SM1). As soon as a photo is taken with a smartphone, it is transferred wirelessly to a cloud server. The server detects the uploaded image and analyzes it against the color profile database. These results can be shared through a variety of methods using hand-held or wearable devices (*i.e.*, smartwatch, smartphone, and smartglasses). For example, we developed an automatic notification system for users to send out a SMS text message and an email of the sensing results (Figure 5b). This system also has the capabilty to post the results onto other social media platforms (*i.e.*, Twitter) and to incorporate temporal information in addition to sparial data derived from Google Maps (data not shown). Our sensor and analysis system can be easily extended to the analysis of many chemicals through further development of specifically engineered M13 phage for desired target molecules.

CONCLUSION

We have demonstrated a sensitive and selective colorimetric sensor array developed from engineered a M13 phage and an accompanying smartphone-based sensor analysis system. We developed bundled phage nanostructures in a columnar smectic phase though a surfactant-assisted self-assembly process. The resulting phage color matrices exhibited brilliant colors depending on their bundle diameters. Furthermore, we engineered various cross-responsive receptors onto the phage that enabled color changes in the presence of certain chemical species. We then demonstrated the sensing ability of these phage color sensor arrays in sensitively detecting relative humidity and selectively distinguishing between harmful aromatic molecules. In addition, we developed an automated sensing tool and information-sharing system by combining these sensor arrays with a smartphone network. Through further modification of these phage with new receptors, this phage color sensor system will be increasingly applicable in environmental protection and national security as well as in medical applications in the monitoring of diseases such as asthma or lung cancer.

MATERIALS AND METHODS

M13 Phage Preparation. We used genetically engineered phage with either E, 2E, 3E, 4E, or WHW peptides fused at the N-terminus of the pVIII major coat protein that we have reported previously.[46] Briefly, the desired peptides were inserted between the first and sixth amino acids of the pVIII protein of the wild-type M13KE phage. An inverse polymerase chain reaction cloning method was conducted using a double-stranded M13KE vector, Phusion DNA polymerase (New England Biolabs, Ipswich, MA), and two desired primers.[46] The resulting products were transformed into XL1-Blue competent cells (Agilent Technologies, Santa Clara, CA) *via* electroporation. Transformed bacteria were amplified by bacteria overnight, and the plasmids were purified and sequenced at the DNA sequencing facility at the University of California, Berkeley, CA. The constructed phages were amplified and purified by polyethylene glycol/sodium chloride precipitation. The amplified phage solution was filtered with 0.45 μm pore size membrane. The final buffer in this study was 0.05% v/v Tween20 in 0.25× TBS (12.5 mM Tris, 37.5 mM NaCl, pH 7.5).

Chemical Modification of M13 Phage. We prepared aromatic functional-group-modified phage using carbodiimide chemistry at the N-terminus of wild-type phage. First, benzoic acid (50 mM, Sigma-Aldrich, St. Louis, MO), 1-ethyl-3-(3-(dimethylamino)propyl)-carbodiimide (50 mM, Creosalus, Louisville, KY), and *N*-hydroxysuccinimide (60 mM, Sigma-Aldrich) were reacted in dimethyl sulfoxide (DMSO) at room temperature (RT) for 3 h. The reacted product was diluted 100 times in a stock solution of wild-type M13 phage. During this reaction, the buffer was 10% v/v DMSO in pH 7.5 10 mM phosphate buffer, and the concentration of the phage was 9 mg/mL. The modified phages were then purified by overnight dialysis through a 3500 molecular weight cutoff cassette (ThermoFisher Scientific, Walthan, MA) in pH 7.0 10 mM phosphate buffer. For characterization of benzoic acid modified phage, 10 μL of the chemically modified phage solution (1 mg/mL) was denatured with 1.5 M guanidine hydrochloride for 5 min at RT, purified with a Millipore C18-ZipTip, and characterized with an Applied Biosystems SCIEX TOF 4800 MALDI-TOF mass spectrometer. α-Cyano-4-hydroxycinnamic acid solution (30 mg/mL in 75% v/v acetonitrile, 25% v/v DI water, 0.1% v/v trifluoroacetic acid) was used as the matrix.

Preparation of Structural Color of Phage Thin Films. The phage color sensor matrices are made using a computer-controlled apparatus built in-house and constructed by modifying a syringe pump as reported previously.[46] Gold-coated SiO_2 wafers were vertically dipped into a phage suspension with designated buffered solution conditions and pulled out at designated speeds using the apparatus.

Grazing-Incidence Small-Angle X-ray Scattering. To characterize the nanostructure of the high ordered M13 phage films, we conducted GISAXS experiments. The GISAXS data were performed at the 7.3.3 beamline in the Advanced Light Source, Lawrence Berkeley National Laboratory. X-rays with a wavelength of 1.24 Å (10 keV) were used, and the scattering spectra were collected on an ADSC Quantum 4 μm CCD detector with an active area of 188 mm × 188 mm (2304 × 2304 pixels). The scattering profiles were obtained after a 10−20 s collection time by integrating the 2D scattering pattern. The sample to detector distance was 1.5 m, and the incidence angle was varied between 0.12 and 0.16° to achieve the best intensity. Line-averaged intensities were reported as I *versus* q, where $q = (4\pi/\lambda) \times \sin(\theta/2)$; λ was the wavelength of incident X-rays, and θ was the scattering angle.

Gas-Sensing Experimental Procedure. We developed a sensor experimental setup that incorporates the phage sensor and an analysis system within an aluminum cell for real-time chemical sensing. The top of the cell was replaced with 2.54 mm thick cast acrylic see-through glass to allow for unobstructed imaging while preventing interactions between the sensor environment and the imaging system. The outer dimensions of this container were 10.2 cm × 3.8 cm × 2.5 cm, and the inner dimensions were 8.9 cm × 2.5 cm × 1.7 cm. Considering that the sensor itself was roughly 1 cm^2 × 1 mm in size, the cell was comparatively large, and this was intended to enable faster and easier sensor replacement. The cell featured one inlet and one outlet that could be fit with 0.64 cm brass tube-to-male pipe fittings. An imaging platform was constructed specifically for sensor testing in real time using a USB CCD camera with simple LED lighting (Celestron LLC, Torrance, CA). A MATLAB script (Mathworks Inc., Natick, MA) was used to control the camera settings to the parameters set to prevent any color drifting caused by the imaging system. A reference gray card was placed immediately beside the phage sensor for color calibration. The script was modified to perform real-time readout by processing captured images and displaying the real-time RGB data. The change in the average RGB values with respect to a reference image for each selected region of interest was calculated in real time.

Four phage-based humidity sensors were used to test various humidity levels. First, dry gas was passed through a dehumidifier in order to filter out most humidity and debris. The gas was then split to two streams controlled by flow meters. One stream entered a humidifier system to elevate the humidity to 100% RH, while the other stream remained dry. By controlling the ratio between these two streams with mass-flow controllers, a wide range of % RH was controlled. To avoid humidity shock and condensation effects, an upper bound of 90% RH was used. The imaging system continuously imaged and analyzed the color response as the humidity was varied while a commercial hygrometer (610, Testo, Wilmington, NC) monitored the humidity level and temperature. These values were

DOI: 10.1021/acsnano.6b07942
ACS Nano 2017, 11, 3632−3641

recorded with the corresponding sensor responses obtained using the MATLAB script. For initial characterization, the humidity was ramped 5% RH every 5 min.

For selective detection of benzene, toluene, xylene, and aniline, approximately 100 μL of the each liquid chemical was deposited on a piece of filter paper that was placed in the sealed experimental cell alongside the phage sensor array. As controls, ambient air, hexane, and methanol were used. Enough chemical was added to the paper so that the vapor in the closed system would be saturated at equilibrium. In addition, we also performed experiments in mixed vapors of methanol, hexane, and each of the individual targets (*i.e.*, BTXA) to test the specificity of our phage sensor in the presence of interfering molecules. In order to expose our films to hexane and methanol, a volume of solvent needed to achieve 10 000 ppm concentration was injected into the chamber with syringe-pump-controlled needles. After equilibration, the changes in RGB values of each phage matrix were recorded quantitatively as described previously. Tests for determining the reproducibility of the phage color pattern generation were carried out in triplicate. The PCA was conducted for statistical analysis using MATLAB. In PCA, the eigenvector is the direction of a newly transformed axis. The eigenvector with the highest eigenvalue is the first principal component. The eigenvalue of each principal component represents the level of dispersion (variance) in response data of sensor along each principal component. RGB values of all array were converted into a dot product with the PCA coefficient matrix with the corresponding principal component value and transform into *xy* coordinates in the PCA space. For the xylene gas exposure experiment, we used two different setups. In order to conduct the phage color sensing experiment with relatively low level of gas exposure, the 0−100 ppm xylene concentrations were prepared by mixing a stream of gas chromatography calibrated xylene with dry and humidified nitrogen gases using digital mass-flow controllers (MKS instruments, Andover, MA) to compose the desired concentrations of xylene with constant 45% RH (Supporting Information Figure S4). For higher level of gas exposure, the desired concentrations (300, 500, 1000, 2000, and 4000 ppm) of xylene were prepared by accurate injections of saturated xylene vapor in a gas-tight syringe (Hamilton, Reno, NV) using a programmable syringe pump (kdScienctific, Holliston, MA) to sealed jar (volume: 190, 520 mL). The top of the jar was covered with glass to allow for imaging and analysis. As previously described, a computer script was written to process captured images and display the real-time RGB data. The average RGB values of selected area for each 10 phage color arrays with respect to a reference gray card were calculated. The minimum color difference (sum of absolute values of each RGB difference in 10 phage color arrays) required to detect xylene was assumed to be three standard deviations from baseline noise in the absence of xylene (Supporting Information Figure S13a). The phage array color difference of 5 ppm xylene could be detectable based on this approach. The color difference from 10 phage color arrays was plotted as a function of xylene concentration (Supporting Information Figure S13b,c). Error bars for data points represent the standard deviation from three independent trials for the test condition.

Smartphone-Based Color Sensor Analysis. We designed a full sensing analysis system that couples our phage color sensor arrays with a smartphone and cloud server. We used the Dropbox app to automatically move photos captured with Android or iOS smartphones to a folder stored on Dropbox. Then, a Python script was used to detect that a new photo was uploaded and begin MATLAB analysis. The new file was identified by comparing the date added fields across all files in that directory and choosing the youngest one.

Our MATLAB script imports the target photo and quantitatively analyzes the RGB values across the phage sensor array. The program converts these RGB values into a dot product using a PCA coefficient matrix with the corresponding principal component value and transforms them into $x-y$ coordinates in PCA space. These coordinates are compared against a database that contains the results from various previously analyzed reference images. The program identifies which of these references are most similar to the active photo by finding the Euclidean distances between their locations in PCA space and choosing the closest two—the two chosen images often represent adjacent concentrations of the target analyte (*e.g.*, 80 and 85% RH would be a logical pair, suggesting that the concentration of the active image falls between these two concentrations). Then, based on how similar the active image is to each of these two references, the concentration of the active image was estimated by interpolation, using the assumption that concentration varies linearly along the line between the two reference points.

The MATLAB results were output to Python, which was used to disseminate information about the sensor array *via* text message, e-mail, or on social media (*i.e.*, Twitter or Facebook). By reading the photo metadata, spatiotemporal information such as the time the photo was taken or the location of the sensor can also be shared.

ASSOCIATED CONTENT

Supporting Information

The Supporting Information is available free of charge on the ACS Publications website at DOI: 10.1021/acsnano.6b07942.

Additional supporting Figures S1−S14 and Table S1 (PDF)

Movie SM1 (AVI)

AUTHOR INFORMATION

Corresponding Author

*E-mail: leesw@berkeley.edu.

ORCID

Ju Hun Lee: 0000-0001-7222-0510

Seung-Wuk Lee: 0000-0002-0501-8432

Notes

The authors declare no competing financial interest.

ACKNOWLEDGMENTS

We acknowledge the funding support by International Cooperative Research Program (No. 5111F5-911148001) from the Agency for Defense Development and Defense Acquisition Program Administration of Korea, Samsung Electronics' Global Research Outreach Program, National Science Foundation STTR phase I grant (No. 1521497), Tsinghua-Berkeley Shenzhen Institute and Waveguider Co., TBSI-Waveguider Joint Lab and Shenzhen Engineering Laboratory for Data Science and Information Technology, Grant Number: SDRC [2015]1872. H.-E.J. was supported by the National Research Foundation of Korea (NRF) grant funded by the Korea government (MSIP) (NRF-2016R1C1B1008824). For GiSAXS measurement, beamline 7.3.3 of the Advanced Light Source is supported by the Director of the Office of Science, Office of Basic Energy Sciences, of the U.S. Department of Energy under Contract No. DE-AC02-05CH11231. Work at the Molecular Foundry was supported by the Office of Science, Office of Basic Energy Sciences, Office of the U.S. Department of Energy under Contract No. DE-AC02-05CH11231.

REFERENCES

(1) Elosua, C.; Matias, I. R.; Bariain, C.; Arregui, F. J. Volatile Organic Compound Optical Fiber Sensors: A Review. *Sensors* **2006**, *6*, 1440−1465.

(2) Chen, X. P.; Wong, C. K. Y.; Yuan, C. A.; Zhang, G. Q. Nanowire-Based Gas Sensors. *Sens. Actuators, B* **2013**, *177*, 178−195.

(3) Pandey, S.; Goswami, G. K.; Nanda, K. K. Nanocomposite Based Flexible Ultrasensitive Resistive Gas Sensor for Chemical Reactions Studies. *Sci. Rep.* **2013**, *3*, 2082.

(4) Miller, D. R.; Akbar, S. A.; Morris, P. A. Nanoscale Metal Oxide-Based Heterojunctions for Gas Sensing: A Review. *Sens. Actuators, B* **2015**, *211*, 569−569.
(5) Dickinson, T. A.; White, J.; Kauer, J. S.; Walt, D. R. Current Trends in 'Artificial-Nose' Technology. *Trends Biotechnol.* **1998**, *16*, 250−258.
(6) Krautwurst, D.; Yau, K. W.; Reed, R. R. Identification of Ligands for Olfactory Receptors by Functional Expression of a Receptor Library. *Cell* **1998**, *95*, 917−926.
(7) Vincent, S. R.; Kimura, H. Histochemical Mapping of Nitric-Oxide Synthase in the Rat-Brain. *Neuroscience* **1992**, *46*, 755−784.
(8) Graziadei, P. P. C.; Graziadei, G. A. M. Neurogenesis and Neuron Regeneration in the Olfactory System of Mammals. I. Morphological Aspects of Differentiation and Structural Organization of the Olfactory Sensory Neurons. *J. Neurocytol.* **1979**, *8*, 1−18.
(9) Jones, D. T.; Reed, R. R. Golf - an Olfactory Neuron Specific G-Protein Involved in Odorant Signal Transduction. *Science* **1989**, *244*, 790−795.
(10) Shepherd, G. M. Outline of a Theory of Olfactory Processing and Its Relevance to Humans. *Chem. Senses* **2005**, *30*, I3−I5.
(11) Buck, L.; Axel, R. A Novel Multigene Family May Encode Odorant Receptors. *J. Gen. Physiol.* **1991**, *98*, A3−A3.
(12) Baik, J. M.; Zielke, M.; Kim, M. H.; Turner, K. L.; Wodtke, A. M.; Moskovits, M. Tin-Oxide-Nanowire-Based Electronic Nose Using Heterogeneous Catalysis as a Functionalization Strategy. *ACS Nano* **2010**, *4*, 3117−3122.
(13) Cole, M.; Covington, J. A.; Gardner, J. W. Combined Electronic Nose and Tongue for a Flavour Sensing System. *Sens. Actuators, B* **2011**, *156*, 832−839.
(14) Sysoev, V. V.; Strelcov, E.; Sommer, M.; Bruns, M.; Kiselev, I.; Habicht, W.; Kar, S.; Gregoratti, L.; Kiskinova, M.; Kolmakov, A. Single-Nanobelt Electronic Nose: Engineering and Tests of the Simplest Analytical Element. *ACS Nano* **2010**, *4*, 4487−4494.
(15) Rock, F.; Barsan, N.; Weimar, U. Electronic Nose: Current Status and Future Trends. *Chem. Rev.* **2008**, *108*, 705−725.
(16) Albert, K. J.; Lewis, N. S.; Schauer, C. L.; Sotzing, G. A.; Stitzel, S. E.; Vaid, T. P.; Walt, D. R. Cross-Reactive Chemical Sensor Arrays. *Chem. Rev.* **2000**, *100*, 2595−2626.
(17) Kreno, L. E.; Leong, K.; Farha, O. K.; Allendorf, M.; Van Duyne, R. P.; Hupp, J. T. Metal-Organic Framework Materials as Chemical Sensors. *Chem. Rev.* **2012**, *112*, 1105−1125.
(18) Minami, T.; Emami, F.; Nishiyabu, R.; Kubo, Y.; Anzenbacher, P. Quantitative Analysis of Modeled ATP Hydrolysis in Water by a Colorimetric Sensor Array. *Chem. Commun.* **2016**, *52*, 7838−7841.
(19) Jia, M.-Y.; Wu, Q.-S.; Li, H.; Zhang, Y.; Guan, Y.-F.; Feng, L. The Calibration of Cellphone Camera-Based Colorimetric Sensor Array and Its Application in the Determination of Glucose in Urine. *Biosens. Bioelectron.* **2015**, *74*, 1029−1037.
(20) Kwon, H.; Jiang, W.; Kool, E. T. Pattern-Based Detection of Anion Pollutants in Water with DNA Polyfluorophores. *Chem. Sci.* **2015**, *6*, 2575−2583.
(21) Seesaard, T.; Lorwongtragool, P.; Kerdcharoen, T. Development of Fabric-Based Chemical Gas Sensors for Use as Wearable Electronic Noses. *Sensors* **2015**, *15*, 1885−1902.
(22) Lichtenstein, A.; Havivi, E.; Shacham, R.; Hahamy, E.; Leibovich, R.; Pevzner, A.; Krivitsky, V.; Davivi, G.; Presman, I.; Elnathan, R.; et al. Supersensitive Fingerprinting of Explosives by Chemically Modified Nanosensors Arrays. *Nat. Commun.* **2014**, *5*, 4195.
(23) Liu, Y. L.; Minami, T.; Nishiyabu, R.; Wang, Z.; Anzenbacher, P. Sensing of Carboxylate Drugs in Urine by a Supramolecular Sensor Array. *J. Am. Chem. Soc.* **2013**, *135*, 7705−7712.
(24) Lim, S. H.; Feng, L.; Kemling, J. W.; Musto, C. J.; Suslick, K. S. An Optoelectronic Nose for the Detection of Toxic Gases. *Nat. Chem.* **2009**, *1*, 562−567.
(25) Carey, J. R.; Suslick, K. S.; Hulkower, K. I.; Imlay, J. A.; Imlay, K. R. C.; Ingison, C. K.; Ponder, J. B.; Sen, A.; Wittrig, A. E. Rapid Identification of Bacteria with a Disposable Colorimetric Sensing Array. *J. Am. Chem. Soc.* **2011**, *133*, 7571−7576.
(26) Mannoor, M. S.; Zhang, S. Y.; Link, A. J.; McAlpine, M. C. Electrical Detection of Pathogenic Bacteria *via* Immobilized Antimicrobial Peptides. *Proc. Natl. Acad. Sci. U. S. A.* **2010**, *107*, 19207−19212.
(27) Haes, A. J.; Chang, L.; Klein, W. L.; Van Duyne, R. P. Detection of a Biomarker for Alzheimer's Disease from Synthetic and Clinical Samples Using a Nanoscale Optical Biosensor. *J. Am. Chem. Soc.* **2005**, *127*, 2264−2271.
(28) Turner, A. P. F.; Magan, N. Electronic Noses and Disease Diagnostics. *Nat. Rev. Microbiol.* **2004**, *2*, 161−166.
(29) Burgess, I. B.; Koay, N.; Raymond, K. P.; Kolle, M.; Loncar, M.; Aizenberg, J. Wetting in Color: Colorimetric Differentiation of Organic Liquids with High Selectivity. *ACS Nano* **2012**, *6*, 1427−1437.
(30) Guo, L.; Yang, Z.; Dou, X. Artificial Olfactory System for Trace Identification of Explosive Vapors Realized by Optoelectronic Schottky Sensing. *Adv. Mater.* **2017**, *29*, 1604528.
(31) Potyrailo, R. A.; Bonam, R. K.; Hartley, J. G.; Starkey, T. A.; Vukusic, P.; Vasudev, M.; Bunning, T.; Naik, R. R.; Tang, Z. X.; Palacios, M. A.; et al. Towards Outperforming Conventional Sensor Arrays with Fabricated Individual Photonic Vapour Sensors Inspired by Morpho Butterflies. *Nat. Commun.* **2015**, *6*, 7959.
(32) Askim, J. R.; Mahmoudi, M.; Suslick, K. S. Optical Sensor Arrays for Chemical Sensing: The Optoelectronic Nose. *Chem. Soc. Rev.* **2013**, *42*, 8649−8682.
(33) Diehl, K. L.; Anslyn, E. V. Array Sensing Using Optical Methods for Detection of Chemical and Biological Hazards. *Chem. Soc. Rev.* **2013**, *42*, 8596−8611.
(34) Furton, K. G.; Myers, L. J. The Scientific Foundation and Efficacy of the Use of Canines as Chemical Detectors for Explosives. *Talanta* **2001**, *54*, 487−500.
(35) Jezierski, T.; Adamkiewicz, E.; Walczak, M.; Sobczynska, M.; Gorecka-Bruzda, A.; Ensminger, J.; Papet, E. Efficacy of Drug Detection by Fully-Trained Police Dogs Varies by Breed, Training Level, Type of Drug and Search Environment. *Forensic Sci. Int.* **2014**, *237*, 112−118.
(36) Smith, G. P. Filamentous Fusion Phage - Novel Expression Vectors That Display Cloned Antigens on the Virion Surface. *Science* **1985**, *228*, 1315−1317.
(37) Smith, G. P.; Petrenko, V. A. Phage Display. *Chem. Rev.* **1997**, *97*, 391−410.
(38) Lee, S. W.; Mao, C. B.; Flynn, C. E.; Belcher, A. M. Ordering of Quantum Dots Using Genetically Engineered Viruses. *Science* **2002**, *296*, 892−895.
(39) Merzlyak, A.; Indrakanti, S.; Lee, S. W. Genetically Engineered Nanofiber-Like Viruses for Tissue Regenerating Materials. *Nano Lett.* **2009**, *9*, 846−852.
(40) Lee, J. H.; Domaille, D. W.; Cha, J. N. Amplified Protein Detection and Identification through DNA-Conjugated M13 Bacteriophage. *ACS Nano* **2012**, *6*, 5621−5626.
(41) Lee, J. H.; Xu, P. F.; Domaille, D. W.; Choi, C.; Jin, S.; Cha, J. N. M13 Bacteriophage as Materials for Amplified Surface Enhanced Raman Scattering Protein Sensing. *Adv. Funct. Mater.* **2014**, *24*, 2079−2084.
(42) Merzlyak, A.; Lee, S. W. Engineering Phage Materials with Desired Peptide Display: Rational Design Sustained through Natural Selection. *Bioconjugate Chem.* **2009**, *20*, 2300−2310.
(43) Krag, D. N.; Shukla, G. S.; Shen, G. P.; Pero, S.; Ashikaga, T.; Fuller, S.; Weaver, D. L.; Burdette-Radoux, S.; Thomas, C. Selection of Tumor-Binding Ligands in Cancer Patients with Phage Display Libraries. *Cancer Res.* **2006**, *66*, 7724−7733.
(44) Muzard, J.; Platt, M.; Lee, G. U. M13 Bacteriophage-Activated Superparamagnetic Beads for Affinity Separation. *Small* **2012**, *8*, 2403−2411.
(45) Lee, J. H.; Jin, H. E.; Desai, M. S.; Ren, S.; Kim, S.; Lee, S. W. Biomimetic Sensor Design. *Nanoscale* **2015**, *7*, 18379−18391.
(46) Chung, W. J.; Oh, J. W.; Kwak, K.; Lee, B. Y.; Meyer, J.; Wang, E.; Hexemer, A.; Lee, S. W. Biomimetic Self-Templating Supramolecular Structures. *Nature* **2011**, *478*, 364−368.

DOI: 10.1021/acsnano.6b07942
ACS Nano 2017, 11, 3632−3641

(47) Potyrailo, R. A.; Ghiradella, H.; Vertiatchikh, A.; Dovidenko, K.; Cournoyer, J. R.; Olson, E. Morpho Butterfly Wing Scales Demonstrate Highly Selective Vapour Response. *Nat. Photonics* **2007**, *1*, 123−128.
(48) Oh, J. W.; Chung, W. J.; Heo, K.; Jin, H. E.; Lee, B. Y.; Wang, E.; Zueger, C.; Wong, W.; Meyer, J.; Kim, C.; et al. Biomimetic Virus-Based Colourimetric Sensors. *Nat. Commun.* **2014**, *5*, 3043.
(49) Grelet, E. Hexagonal Order in Crystalline and Columnar Phases of Hard Rods. *Phys. Rev. Lett.* **2008**, *100*, 168301.
(50) Dogic, Z.; Fraden, S. Ordered Phases of Filamentous Viruses. *Curr. Opin. Colloid Interface Sci.* **2006**, *11*, 47−55.
(51) Young, K. L.; Jones, M. R.; Zhang, J.; Macfarlane, R. J.; Esquivel-Sirvent, R.; Nap, R. J.; Wu, J. S.; Schatz, G. C.; Lee, B.; Mirkin, C. A. Assembly of Reconfigurable One-Dimensional Colloidal Superlattices Due to a Synergy of Fundamental Nanoscale Forces. *Proc. Natl. Acad. Sci. U. S. A.* **2012**, *109*, 2240−2245.
(52) Adams, M. E.; Dogic, Z.; Keller, S. L.; Fraden, S. Entropically Driven Microphase Transitions in Mixtures of Colloidal Rods & Spheres. *Abstr. Pap. Am. Chem. S.* **1998**, *216*, U643−U643.
(53) Buzzaccaro, S.; Piazza, R.; Colombo, J.; Parola, A. Enhancement of Depletion Forces by Electrostatic Depletant Repulsion. *J. Chem. Phys.* **2010**, *132*, 124902.
(54) Bonard, J. M.; Stora, T.; Salvetat, J. P.; Maier, F.; Stockli, T.; Duschl, C.; Forro, L.; deHeer, W. A.; Chatelain, A. Purification and Size-Selection of Carbon Nanotubes. *Adv. Mater.* **1997**, *9*, 827−831.
(55) Chen, Z.; Lu, C. Humidity Sensors: A Review of Materials and Mechanisms. *Sens. Lett.* **2005**, *3*, 274−295.
(56) Mogera, U.; Sagade, A. A.; George, S. J.; Kulkarni, G. U. Ultrafast Response Humidity Sensor Using Supramolecular Nanofibre and Its Application in Monitoring Breath Humidity and Flow. *Sci. Rep.* **2014**, *4*, 4103.
(57) Janzen, M. C.; Ponder, J. B.; Bailey, D. P.; Ingison, C. K.; Suslick, K. S. Colorimetric Sensor Arrays for Volatile Organic Compounds. *Anal. Chem.* **2006**, *78*, 3591−3600.
(58) Santiago, F.; Alves, G.; Otero, U. B.; Tabalipa, M. M.; Scherrer, L. R.; Kosyakova, N.; Ornellas, M. H.; Liehr, T. Monitoring of Gas Station Attendants Exposure to Benzene, Toluene, Xylene (BTX) Using Three-Color Chromosome Painting. *Mol. Cytogenet.* **2014**, *7*, 15.
(59) Wang, L.; Barrington, S.; Kim, J. W. Biodegradation of Pentyl Amine and Aniline from Petrochemical Wastewater. *J. Environ. Manage.* **2007**, *83*, 191−197.
(60) Li, K.; Chen, Y.; Li, S. Q.; Nguyen, H. G.; Niu, Z. W.; You, S. J.; Mello, C. M.; Lu, X. B.; Wang, Q. A. Chemical Modification of M13 Bacteriophage and Its Application in Cancer Cell Imaging. *Bioconjugate Chem.* **2010**, *21*, 1369−1377.
(61) Laurent, G. Olfactory Network Dynamics and the Coding of Multidimensional Signals. *Nat. Rev. Neurosci.* **2002**, *3*, 884−895.
(62) Gschwend, O.; Abraham, N. M.; Lagier, S.; Begnaud, F.; Rodriguez, I.; Carleton, A. Neuronal Pattern Separation in the Olfactory Bulb Improves Odor Discrimination Learning. *Nat. Neurosci.* **2015**, *18*, 1474−1482.

DOI: 10.1021/acsnano.6b07942
ACS Nano 2017, 11, 3632−3641